

Fretting wear of bolted joint interfaces

*Original*

Fretting wear of bolted joint interfaces / Li, Dongwu; Botto, Daniele; Xu, Chao; Gola, Muzio. - In: WEAR. - ISSN 0043-1648. - ELETTRONICO. - 458-459:(2020), p. 203411. [10.1016/j.wear.2020.203411]

*Availability:*

This version is available at: 11583/2843468 since: 2020-08-31T12:10:35Z

*Publisher:*

Elsevier

*Published*

DOI:10.1016/j.wear.2020.203411

*Terms of use:*

This article is made available under terms and conditions as specified in the corresponding bibliographic description in the repository

*Publisher copyright*

Elsevier postprint/Author's Accepted Manuscript

© 2020. This manuscript version is made available under the CC-BY-NC-ND 4.0 license  
<http://creativecommons.org/licenses/by-nc-nd/4.0/>. The final authenticated version is available online at:  
<http://dx.doi.org/10.1016/j.wear.2020.203411>

(Article begins on next page)

## Fretting wear of bolted joint interfaces

Dongwu Li<sup>1</sup>, Daniele Botto<sup>2</sup>, Chao Xu<sup>1, 3\*</sup>, Muzio Gola<sup>2</sup>

<sup>1</sup>*School of Astronautics, Northwestern Polytechnical University, Xi'an 710072, China*

<sup>2</sup>*Department of Mechanical and Aerospace Engineering, Politecnico di Torino, Turin 10129, Italy*

<sup>3</sup>*Qingdao R&D Institute, Northwestern Polytechnical University, Qingdao, 266200, China*

**Abstract:** Under vibration loading, fretting wear between bolted joint interfaces may change the dynamic characteristics of structures. Even the reliability of long-lasting assembly structures could be affected. This paper focuses on an experimental study on the fretting wear behavior of bolted joint interfaces under tangential loading. A recently developed fretting test apparatus was used to measure the hysteresis loops and the bolt preload at different fretting wear cycles. Changes of tangential contact stiffness and friction coefficient were estimated from the measured hysteresis loops. Experimental results showed a large change in bolt preload, contact stiffness, and friction coefficient due to fretting wear. The effect of surface roughness on fretting wear behavior of bolted joint interfaces was discussed. A modified Iwan model, comprehensive of wear effects, was proposed to simulate the hysteresis loops. Comparison between simulations and experimental results was performed to validate the proposed method. Results achieved in this research can provide the basis for the dynamic analysis of long-lasting joint structures in which wear plays a fundamental role in modifying the contact parameters.

**Keywords:** Fretting wear; bolted joint; hysteresis loop; contact parameters; Iwan model.

---

\*Corresponding author: [chao\\_xu@nwpu.edu.cn](mailto:chao_xu@nwpu.edu.cn)

Address: No. 127 Youyi West Road, Xi'an, Shaanxi 710072, China

## 1 Introduction

Bolted joints are widely used in mechanical assemblies. Connected parts are brought into contact by bolt preload and transmit tangential loads by dry friction. Under oscillating loading, the contact interfaces may undergo a relative motion with a small amplitude, which is referred to as fretting. There are two main drawbacks associated with fretting: fretting fatigue and fretting wear. Roughly speaking, fretting fatigue is associated with small relative displacements (micro-slip regime), whereas fretting wear involves large relative displacements (gross slip regime). Fretting fatigue of bolted joints is outside the scope of this article but it was studied in many papers[1-3]. The tangential friction force plotted as a function of the relative displacement between the contact surfaces give the hysteresis loop. This relationship exhibits a nonlinear behavior [4-6]. The area enclosed by the loop is the friction-induced energy dissipation.

Increasing fretting wear cycles leads to material removal and change in interface topography. Therefore, the contact behavior is modified because the contact stiffness and the friction-induced damping varies with the fretting wear cycles. These changes significantly affect the dynamic characteristics of joint structures [7-10]. At present, modeling fretting wear and its effects on the dynamics of mechanical systems is becoming a major challenge in the field of the jointed structures.

A very good understanding of the physical phenomena associated with fretting wear helps in modeling the behavior of joint interfaces. Yoon et al. [11] experimentally studied fretting wear in a spherical contact subjected to constant normal load and measured the evolution of hysteresis loops. The results revealed that the shape of hysteresis loops changed as a function of the number of fretting cycles: the amplitude of relative displacement gradually decreased and the tangential force at the gross slip stage increased. The dissipated energy per cycle increased in the first 500 cycles and then it levelled off. Other similar results can be found in the literature [12, 13]. Fantetti et al. [8] measured the hysteretic properties of a flat-on-flat contact pair and studied the effect of fretting wear on structural dynamics. They replicated the evolution of hysteresis loops using a modified Bouc-Wen model incorporating contact parameters evolution. Eriten et al. [14] investigated the effects of surface roughness and lubrication on hysteresis loops at the early stage of the fretting of bolted joints. They

119  
120  
121  
122 found the surface roughness influenced the shape of fretting loops and dissipated energy per cycle.  
123  
124 Lavella et al. [15-17] developed a flat-on-flat fretting test rig with high-temperature capability and  
125  
126 studied the effect of temperature on wear behavior. The results showed a significant dependence of the  
127  
128 hysteresis loops on the temperature.

129  
130 Two contact parameters, namely the friction coefficient and the tangential contact stiffness, can  
131  
132 be used to replicate the hysteresis loop. Fretting wear can lead to significant changes in these  
133  
134 parameters. Almost all experimental studies found that both the friction coefficient and contact  
135  
136 stiffness rapidly increased during a running-in period [8, 11, 15, 18-23]. This trend was explained with  
137  
138 the interlocking between protrusions and depressions on the contact surfaces [19, 20]. As the wear  
139  
140 process continues, studies showed that the friction coefficient reached a peak, decreased and then  
141  
142 levelled off [20-23]. Other studies showed that the friction coefficient increased approaching a steady  
143  
144 state asymptote [8, 23]. Hintikka et al. [22] pointed out that the slight drop in the friction coefficient  
145  
146 was caused by wear debris. A reason for the stabilization in contact parameters was the balance  
147  
148 between generation and ejection of wear debris [8]. In addition, some works studied the effect of  
149  
150 surface roughness and high temperature on the evolution of contact parameters with increasing wear  
151  
152 [14, 15, 18, 21].

152 All the above-mentioned test cases had a constant normal load. This condition is different from  
153  
154 what we can find in bolted joints in which fretting wear could vary the preload.

155  
156 The objective of this work is to investigate the effect of fretting wear on the behavior of bolted  
157  
158 joints. Fretting tests were performed to capture the evolution of hysteresis loops and of the associated  
159  
160 contact parameters. Tests were carried out using a recently developed fretting test rig. To evaluate the  
161  
162 effect of the bolt preload on the fretting behavior, the preload was monitored and recorded during each  
163  
164 test. The effects of surface roughness and sliding amplitude on fretting response was studied as well.  
165  
166 Moreover, a contact model was put forward to recreate hysteresis loops under different wear conditions.  
167  
168 A novel modified Iwan model, comprehensive of wear effects, was developed to simulate the  
169  
170 hysteresis loops.

171  
172 The aim of these analysis was to promote a better understanding of fretting wear behavior of bolted  
173  
174 joint interfaces and to provide the modeling basis for the dynamic analysis of long-lasting joint  
175  
176  
177

178  
179  
180  
181 structures.

182  
183 The paper is organized as follows. [Section 2](#) briefly describes the fretting test apparatus used in  
184 this test campaign and details the wear test plan. [Section 3](#) shows the evolution of measured hysteresis  
185 loops, bolt preloads and contact parameters with increasing wear cycles. The effects of surface  
186 roughness on wear evolution are also discussed. [Section 4](#) models the evolution of contact parameters  
187 and develops a modified Iwan model to replicate the evolution of hysteresis loops. [Section 5](#) discusses  
188 the experimental findings and highlights the reliability of the numerical method.  
189  
190  
191  
192  
193  
194  
195  
196  
197  
198  
199  
200  
201  
202  
203  
204  
205  
206  
207  
208  
209  
210  
211  
212  
213  
214  
215  
216  
217  
218  
219  
220  
221  
222  
223  
224  
225  
226  
227  
228  
229  
230  
231  
232  
233  
234  
235  
236

237  
238  
239  
240  
241  
242  
243  
244  
245  
246  
247  
248  
249  
250  
251  
252  
253  
254  
255  
256  
257  
258  
259  
260  
261  
262  
263  
264  
265  
266  
267  
268  
269  
270  
271  
272  
273  
274  
275  
276  
277  
278  
279  
280  
281  
282  
283  
284  
285  
286  
287  
288  
289  
290  
291  
292  
293  
294  
295

## 2 Experimental Method

### 2.1 Description of the test apparatus

Experimental tests were conducted using the fretting test apparatus described in [24]. This rig was designed to study friction hysteresis behavior of bolted joint interfaces. Fig. 1 (a) Photographs of the test apparatus, (b) Sketch of the test apparatus and main components. Figure 1 shows the test apparatus and its main components. The joint is displaced by a piezoelectric actuator that moves one of the specimens, denoted as moving specimen, with an oscillating tangential displacement  $\Delta x$ . This displacement induces a tangential friction force at the contact surfaces. This force is measured with a dynamic load cell located at one end of the other specimen, denoted as fixed specimen. The relative displacement is measured by a laser vibrometer whose beam is bent with a prism. The bolt preload is measured with a force washer. Additional details and an accurate description of the working principle of the rig can be found in [24]. The measured contact friction force and the relative displacement give the well-known hysteresis loops. Tangential contact stiffness and friction coefficient can be extracted post-processing these loops.

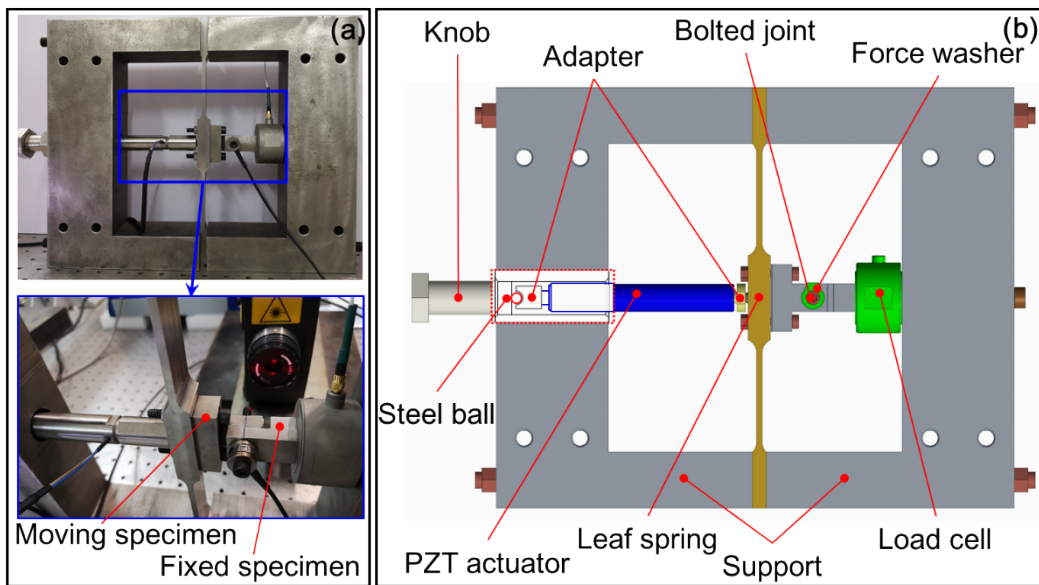


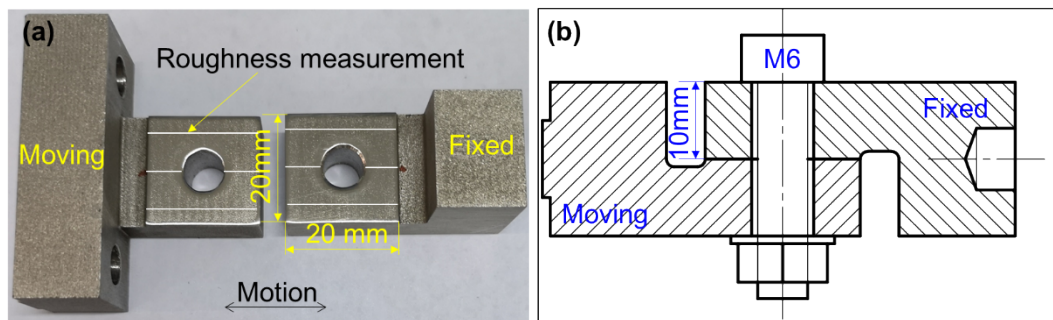
**Fig. 1** (a) Photographs of the test apparatus, (b) Sketch of the test apparatus and main components.

The piezoelectric actuator is closed loop controlled using a built-in strain gauge sensor and a position servo controller. This control ensures the stability of excitation during fretting wear tests. The force-displacement data were continuously measured during the fretting test to monitor the evolution

296  
297  
298  
299 of hysteresis behavior. The tangential contact stiffness and the friction coefficient were extracted from  
300 the hysteresis loops. The evolution of the bolt preload with the number of wear cycles was also  
301 recorded as wear is one of the important reasons why the bolt preload is loosened [24-27].  
302  
303

## 304 2.2 Joint specimens

305  
306 The bolted joint specimens are made of ASTM 304 stainless steel. The nominal contact region is  
307 a 20 mm×20 mm square excluding the 7 mm diameter through hole. In these tests the bolt was an 8.8  
308 M6. Figure 2 shows a photograph and a sketch of the bolted joint specimens.  
309  
310  
311



312  
313  
314  
315  
316  
317  
318  
319  
320  
321  
322 **Fig. 2** (a) Photograph of the joint specimens, (b) Sketch of the joint specimens

323  
324 Joint specimens were manufactured by wire cutting, which leads to a large roughness of the  
325 contact surface. The roughness was measured with a portable roughness profilometer. White lines in  
326 Fig. 2(a) show the measurement paths selected along the sliding direction. The measurement length  
327 was 4 and 2.4 mm on side and central lines, respectively. The average value of the measured roughness  
328 was regarded as the roughness of the contact surface.  
329  
330  
331  
332

333  
334 Specimens were divided into two groups, differing for surface roughness. The contact surfaces of  
335 the first group were carefully hand-polished using two different grades of sandpaper (first 800 grit and  
336 then 1200 grit), leading to a roughness  $R_a$  of about 1  $\mu\text{m}$ . The contact surfaces of the second group of  
337 specimens were not treated, and their roughness  $R_a$  was about 4  $\mu\text{m}$ . Figure 3 shows photographs of  
338 rough (second group) and smooth (first group) surfaces.  
339  
340  
341  
342  
343  
344  
345  
346  
347  
348  
349  
350  
351  
352  
353  
354

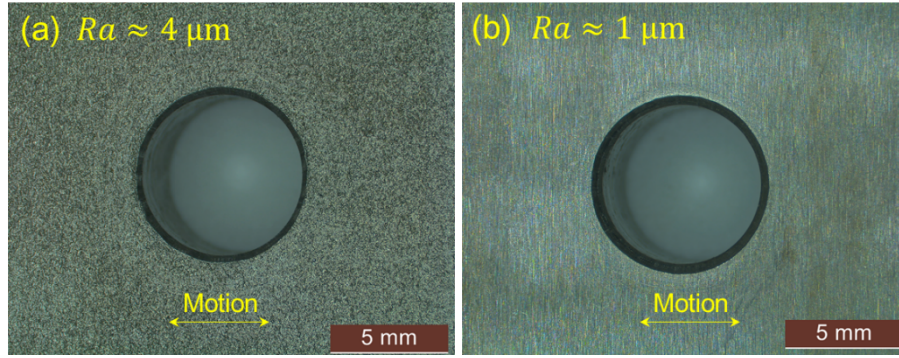


**Fig. 3** Photograph of the contact surfaces and corresponding surface roughness  $R_a$ , (a) rough surface:  $R_a \approx 4 \mu\text{m}$ , (b) smooth surface:  $R_a \approx 1 \mu\text{m}$ .

### 2.3 Wear test plan

Four fretting tests were conducted using different couples of joint specimens. The average roughness of the contact surface of each test specimen is shown in Table 1. Two nominal tangential displacements,  $\Delta x = 50 \mu\text{m}$  and  $40 \mu\text{m}$ , were applied to the contact surfaces. The maximum allowable nominal displacement ( $\Delta x = 70 \mu\text{m}$ ) on the piezoelectric actuator was not applied as an excessive temperature due to long-lasting work could damage the piezoelectric.

**Table 1** Roughness  $R_a$  of the joint specimens for the tests 1/2/3/4, unit in  $\mu\text{m}$

	Test 1	Test 2	Test 3	Test 4
Fixed specimen	4.34	0.78	4.27	0.81
Moving specimen	5.19	0.92	4.43	0.90

Tests were performed at a frequency of 25 Hz, that is far from resonance in the rig, as explained in [24]. The initial bolt preload was about 720 N for all tests, with a 5% scattering among different tests. This preload was chosen because it allowed to reach the selected excitation amplitudes and induce gross slip regime in the joint interface. Working in gross slip regime is a prerequisite for estimating the friction coefficients. Unlike the torque control method, this apparatus directly measures the preload using a force washer, so that the value of the preload can be controlled with great accuracy. The resulting nominal contact pressure was about 2 MPa. All tests were conducted at 25 °C and lasted 12 hours (1.08 million wear cycles). Table 2 summarizes the test specifications and operating conditions.

Data acquisition was performed with an in-house code written in LabVIEW 14.0. All forces and



414 displacements were sampled at 5 kHz, and no filtering was applied. It was impossible to record 100%  
 415 of the data because of the limited memory of the hard disk compared with the large amount of measured  
 416 data. Therefore, the following acquisition strategy was used: for the first 20 minutes, 1-second data  
 417 every 5 seconds was recorded; from 20 to 90 minutes, 1-second data every 40 seconds was recorded;  
 418 from 90 to 720 minutes, 1-second data every 200 seconds was recorded.  
 419  
 420  
 421  
 422  
 423  
 424  
 425

426 **Table 2** Summary of the wear test plan  
 427

	Test 1 / Test 2	Test 3 / Test 4
428 Material	Stainless steel	Stainless steel
429 Roughness, $R_a$	4 $\mu\text{m}$ / 1 $\mu\text{m}$	4 $\mu\text{m}$ / 1 $\mu\text{m}$
430 Excitation amplitude, $\Delta x$	50 $\mu\text{m}$	40 $\mu\text{m}$
431 Excitation frequency, $f$	25 Hz	25 Hz
432 Bolt preload, $N_b$	720 N	720 N
433 Running time	12 hours	12 hours
434 Temperature	25 °C	25 °C

435 Before and after each test, the specimens and the bolt were cleaned with alcohol in an ultrasonic  
 436 bath for 30 min to minimize the effects of particles and machine oil on test results. After cleaning,  
 437 microscopic images of contact surfaces were taken with a Leica S9D stereomicroscope.  
 438  
 439  
 440  
 441  
 442  
 443  
 444  
 445  
 446  
 447  
 448  
 449  
 450  
 451  
 452  
 453  
 454  
 455  
 456  
 457  
 458  
 459  
 460  
 461  
 462  
 463  
 464  
 465  
 466  
 467  
 468  
 469  
 470  
 471  
 472

### 3 Experimental results and discussion

Figure 4 illustrates an example of measured hysteresis loop. The area enclosed by the hysteresis loop represents dissipated energy per cycle. The hysteresis loop can be characterized using two contact parameters: tangential contact stiffness  $k_t$  and friction coefficient  $\mu$ . The tangential contact stiffness is determined by the slope of the force-displacement curve at the stick stage,  $k_t = \Delta T / \Delta \delta$ , see the blue line in Fig. 4. The friction coefficient is usually defined as the ratio between the tangential and the normal force during the gross slip regime. Results showed that the tangential force during the gross slip regime was not constant, as pointed out by the red lines in Fig. 4. This behavior is due to the residual stiffness that is caused by the bending of the bolt shank. A detailed analysis of the residual stiffness was done in [24]. Therefore, the friction coefficient was determined in a different way. The difference between the tangential force during the loading and unloading gross slip regime was  $\Delta T = T_{GS\_load} - T_{GS\_unload}$ . This difference is visualized as the distance between the two red lines in Fig. 4. In the difference  $\Delta T$ , the contribution of the residual stiffness is cancelled. The friction coefficient can be defined as the ratio between  $\Delta T$  and twice the bolt preload,  $\mu = \Delta T / 2N_b$ .

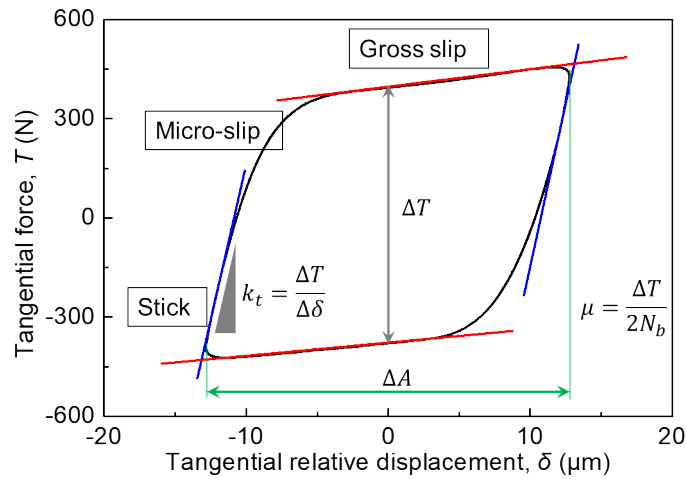


Fig. 4. Typical hysteresis loop and schematic of the contact parameters extraction method.

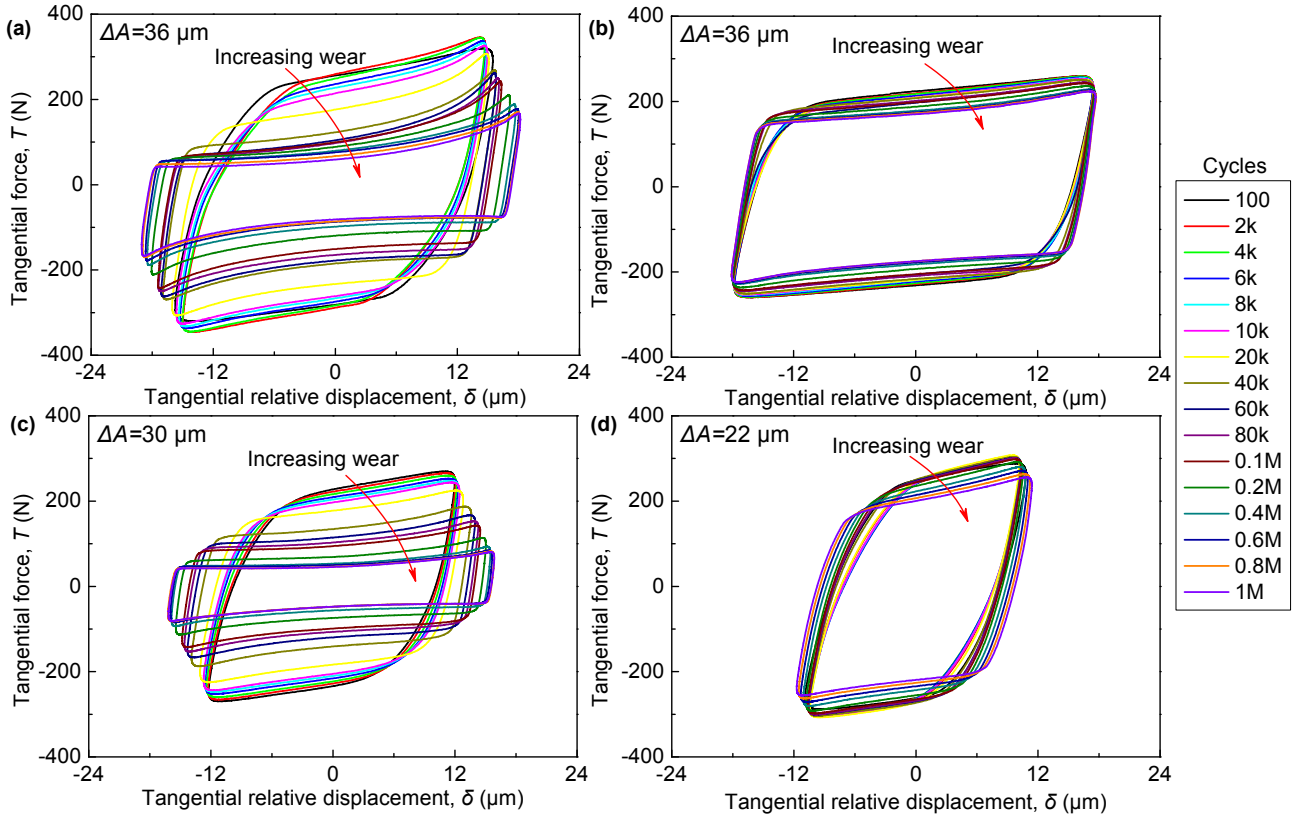
#### 3.1 Evolution of hysteresis loops

Figure 5 shows the evolution of the hysteresis loops during one million wear cycles. The shape of hysteresis loops changed with increasing wear cycle. These changes were due to two main effects. The first effect was the modification of the contact surface and therefore of the friction coefficient and contact stiffness. The second effect was the variation of the bolt preload. Variation in the hysteresis

532  
533  
534 loops was more evident in tests 1 and 3 (specimens with high roughness) than in test 2 and 4 (specimens  
535 with low roughness). As a general trend, the tangential force at the gross slip stage gradually decreases  
536 with increasing the wear cycles. For tests 1 and 2, the average sliding strokes, namely twice the  
537 amplitude  $\delta$ ,  $\Delta A$  were 36  $\mu\text{m}$ ; in test 3 30  $\mu\text{m}$  and in test 4 the average stroke was 22  $\mu\text{m}$ . Rough  
538 surfaces (tests 1 and 3) showed average sliding stroke more scattered than smooth surfaces (tests 2 and  
539 4). [Figure 6](#) shows the normalized hysteresis loops, in which the tangential force was divided by the  
540 bolt preload. The general trend was reversed with respect to the behavior shown in [Fig. 5](#) and the  
541 normalized tangential force increases with the wear cycles. The normalized tangential force is related  
542 to friction coefficient. It will be discussed in section 3.3.

543  
544 An additional phenomenon can be observed in the tests. The force-displacement curve at the end  
545 of the gross slip stage exhibits a bulge – stiffness hardening – after about 0.1 million wear cycles. The  
546 higher the amplitude of the relative displacement, the more evident was the stiffness hardening. This  
547 phenomenon was observed in several wear experiments [15, 20, 23, 28, 29], but the physical reason  
548 was not fully understood yet. There are two possible explanations: (i) interaction among wear scars  
549 that are not present on the new contact surfaces and (ii) the bolt pinning effect, that is, the bolt shank  
550 getting in contact with the through hole.

591  
592  
593  
594  
595  
596  
597  
598  
599  
600  
601  
602  
603  
604  
605  
606  
607  
608  
609  
610  
611  
612  
613  
614  
615  
616  
617  
618  
619  
620  
621  
622  
623  
624  
625  
626  
627  
628  
629  
630  
631  
632  
633  
634  
635  
636  
637  
638  
639  
640  
641  
642  
643  
644  
645  
646  
647  
648  
649



**Fig. 5.** Evolution of hysteresis loops with increasing wear, (a) Test 1:  $\Delta x = 50 \mu\text{m}$ ,  $R_a \approx 4 \mu\text{m}$ , (b) Test 2:  $\Delta x = 50 \mu\text{m}$ ,  $R_a \approx 1 \mu\text{m}$ , (c) Test 3:  $\Delta x = 40 \mu\text{m}$ ,  $R_a \approx 4 \mu\text{m}$ , (d) Test 4:  $\Delta x = 40 \mu\text{m}$ ,  $R_a \approx 1 \mu\text{m}$ .

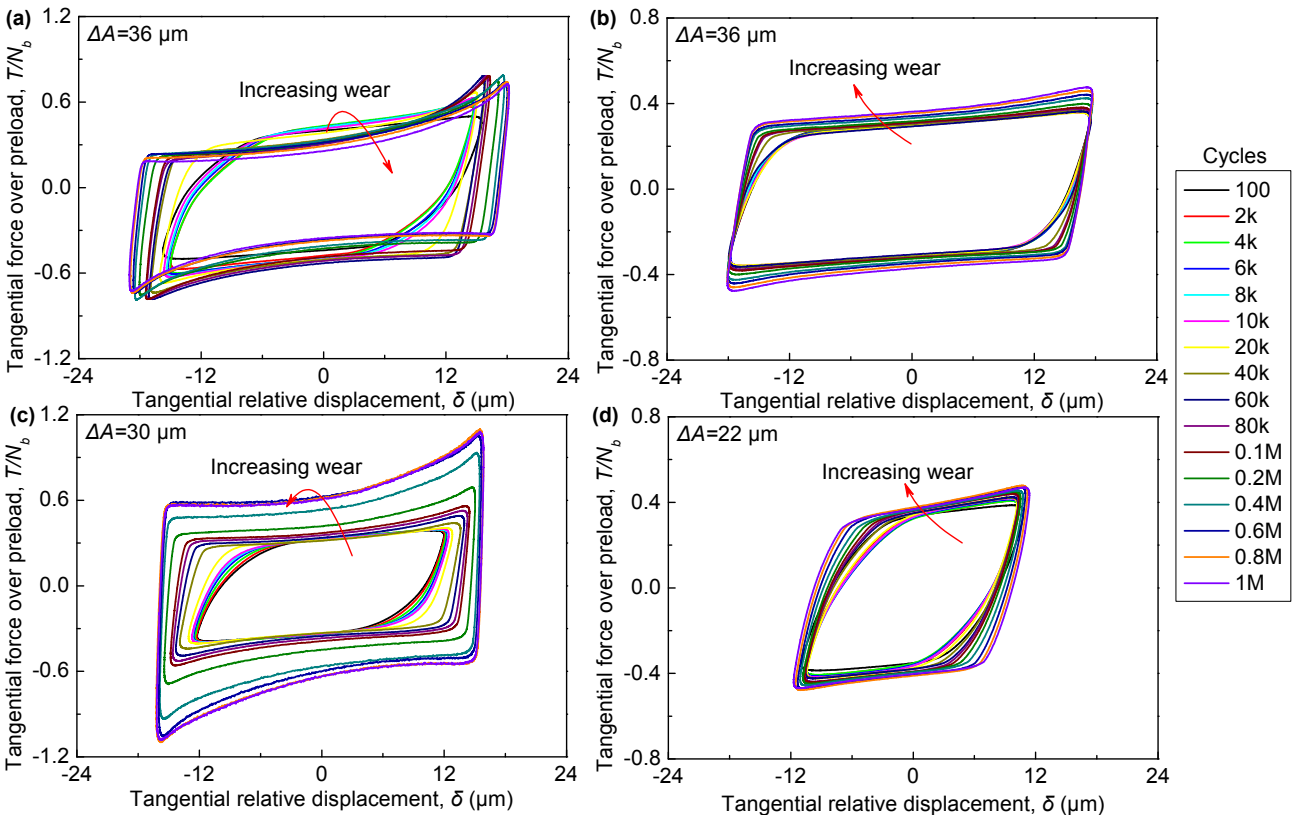


**Fig. 6.** Tangential force versus bolt preload for different tests, (a) Test 1:  $\Delta x = 50 \mu\text{m}$ ,  $R_a \approx 4 \mu\text{m}$ , (b) Test 2:  $\Delta x = 50 \mu\text{m}$ ,  $R_a \approx 1 \mu\text{m}$ , (c) Test 3:  $\Delta x = 40 \mu\text{m}$ ,  $R_a \approx 4 \mu\text{m}$ , (d) Test 4:  $\Delta x = 40 \mu\text{m}$ ,  $R_a \approx 1 \mu\text{m}$ .

Figure 7 plots the evolution of the dissipated energy per cycle  $E_c$  as a function of the cumulative dissipated energy  $E$ . In tests 1 and 3, the dissipated energy per cycle decreased and then gradually stabilized. The dissipated energy in the final state is 42% and 25% of the initial value, respectively. In tests 2 and 4, the dissipated energy showed a short period of oscillation and then gradually reached a steady state. And the change in dissipated energy  $E_c$  was much lower. In test 2, the dissipated energy  $E_c$  in the final state was 84% of the initial value. In test 4, the dissipated energy  $E_c$  almost remained unchangeable after the initial oscillation. The dissipated energy per cycle in tests 2 and 4 (low roughness) was significantly larger than in tests 1 and 3 (high roughness), except for the first thousand cycles.

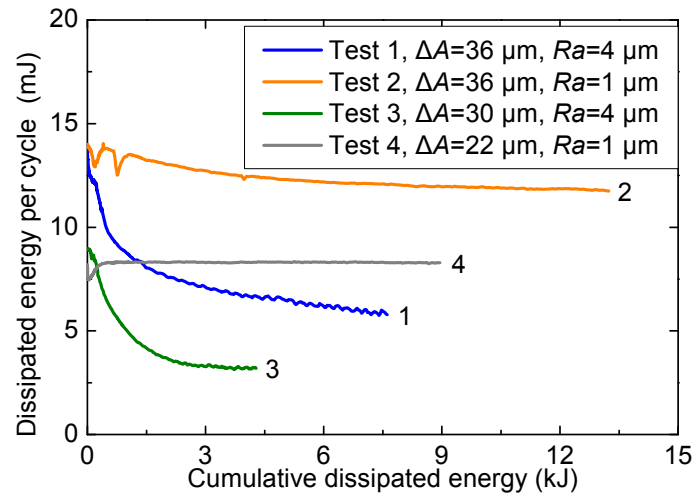


**Fig. 7.** Dissipated energy per cycle for the different tests.

### 3.2 Evolution of bolt preloads

Wear tests are usually performed with a constant normal load [8, 15, 19, 29, 30]. Differently from standard test, in this work the normal load was not constant because the bolt preload varied with wear cycles. Figure 8 illustrates the variation of bolt preloads with the cumulative dissipated energy. In all tests, the bolt preloads showed a trend with a steep descent then it approached to an asymptotic steady-state value.

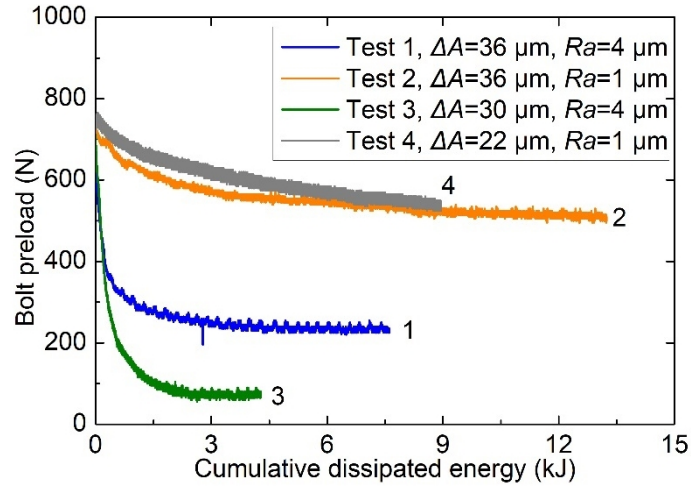


**Fig. 8.** Bolt preloads for the different tests.

Tests performed in this work showed that in tests 1 and 3 the reduction in bolt preload was more than that in tests 2 and 4. Figure 9 depicts the percentage reduction in bolt preload,  $P_r = (N_{b-initial} - N_{b-end}) / N_{b-initial}$ , where  $N_{b-initial}$  represents the initial value of the bolt preload, and  $N_{b-end}$  its final value. The preload reduction was more pronounced for the contact surfaces with higher roughness than for lower roughness. In test 3 the reduction even reached 90% of the initial value while in tests 2 and 4 the preload reduction was less than 30%. The decrease in bolt preload under transversal vibration was widely investigated in the literature. A reasonable explanation of preload loosening is that the peaks of micro-protrusions of rough surfaces are cut and flattened during the wear process. The interference fit between the contact surfaces is reduced, which in turn results in preload decreasing. Experimental results pointed out that rough surfaces experienced greater bolt preload drop off than smooth surfaces. Recent investigations [25] revealed that the main cause of preload loosening at the early stage was the stress release and the redistribution of threaded teeth. In [25] the effect of roughness was not investigated.

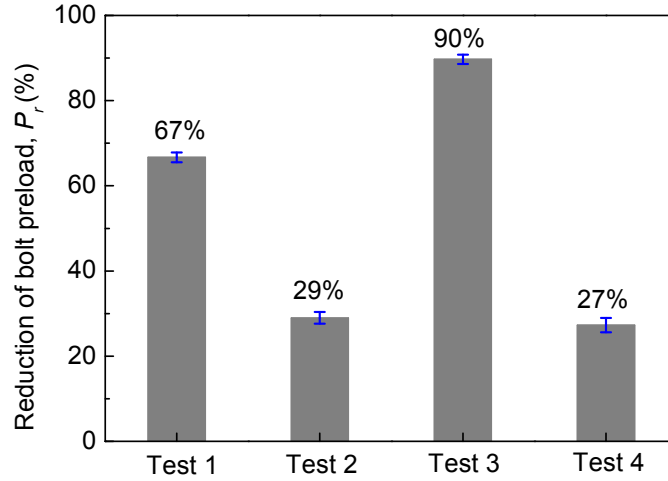


**Fig. 9.** Reduction in bolt preload with respect to the initial value in the four tests,  $P_r=(N_{b-initial} - N_{b-end})/N_{b-initial}$ ,  $N_{b-initial}$  is the initial value of the bolt preload, and  $N_{b-end}$  its final value. The blue bar represents its standard deviation.

### 3.3 Evolution of contact parameters

It is known that the contact stiffness and the friction coefficient are notably affected by the wear of contact surfaces [8, 15, 23]. The contact parameters were computed according to the procedure described in Section 3 and summarized in Fig. 4.

#### 3.3.1 Tangential contact stiffness

Figure 10(a) plots the contact stiffness as a function of the cumulative dissipated energy  $E$ . Results showed a large variation of the contact stiffness. Contact stiffness in test 1 was higher than in test 3 even if they showed a similar behavior: contact stiffness first experienced a rapid and significant increase, reaching a peak at about 13 kJ of dissipated energy, then they decreased. Figure 10(b) presents the contact stiffness as a function of the bolt preload and shows that the contact stiffness increased even if the bolt preload decreases. Several experimental evidences indicate that higher normal load gives higher contact stiffness. On the other hand, theoretical result using the Mindlin solution [31] reveals that the contact stiffness is proportional to the radius of the contact area and does not depend on the normal load, as shown in Eq.(1)

$$k_t = \frac{8Ga}{2 - \nu} \quad (1)$$

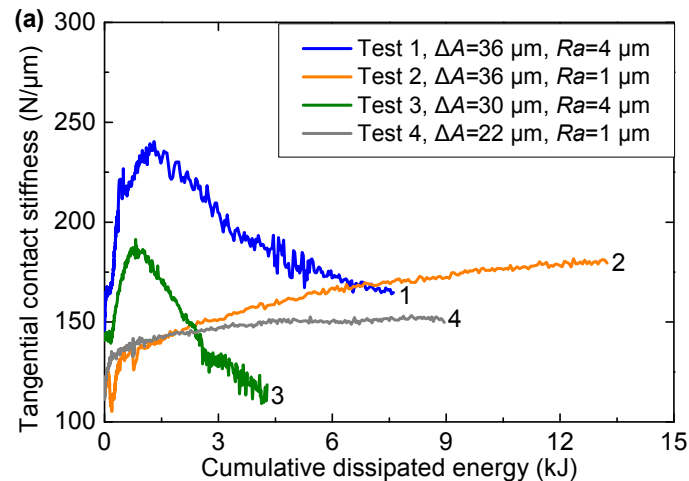
where  $G$ ,  $a$  and  $\nu$  denote shear modulus, radius of the contact area and Poisson's ratio, respectively.

Therefore, the relationship between the normal load and the contact stiffness appears to be related to

827  
828  
829  
830 the change in the contact area: increasing the normal load increases the contact area and therefore the  
831 contact stiffness. In our tests the normal load was variable and diminished with the wear cycles,  
832 therefore, the contact stiffness was expected to decrease. Due of the wear process, the contact area  
833 increased and therefore the contact stiffness also increased.  
834  
835  
836

837 The contact stiffness can also be related to the height of the asperity at the interfaces [8, 19]. The  
838 initial contact stiffness of the rough surfaces (test 1 and test 3) was significantly greater than that of  
839 the smooth surfaces (test 2 and test 4). Therefore, the increase in contact stiffness may be mainly  
840 caused by the increased interaction between wear scars. This interaction increases the resistance to the  
841 relative motion between the contact surfaces at the stick stage. When the bolt preload drops to a certain  
842 level, the preload dominates the change in contact stiffness. This resulted in reduced contact stiffness  
843 after the peak.  
844  
845  
846  
847  
848  
849

850 In tests 2 and 4, the contact stiffness also increased at the early stage of fretting wear, then it  
851 gradually stabilized. The same trend was observed in the experiments reported in [8, 23] where the  
852 normal load was constant during the wear tests and the contact surface roughness was about  $1\ \mu\text{m}$ . In  
853 these experiments, the reduction in bolt preload was negligible, so that modification of the contact  
854 surfaces was the main reason for the variation of the contact stiffness.  
855  
856  
857  
858  
859





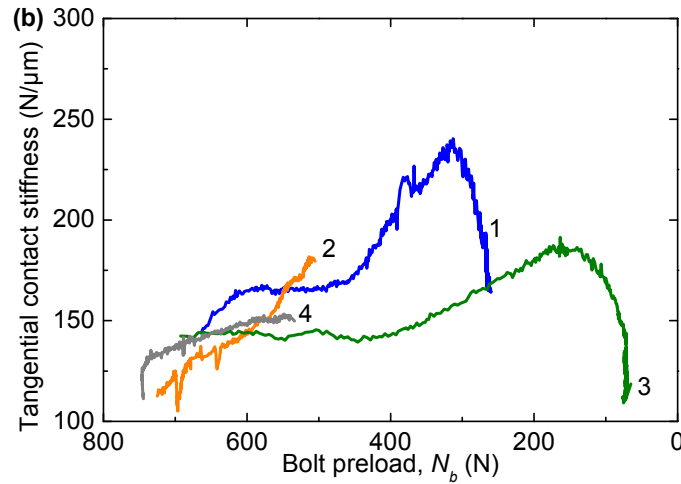


**Fig. 10.** Tangential contact stiffness depending on (a) cumulative dissipated energy, and (b) bolt preload.

### 3.3.2 Friction coefficient

The trend of the friction coefficient for the four tests is shown in Figure 11. Tests 1 and 3 showed a similar trend. In test 1, the friction coefficient increased, it reached the peak and then decreased with evident fluctuations. In test 3, the friction coefficient peaked at about 3 kJ, the peak value (0.6) was about two times the initial value (0.3), then it decreased slowly with evident oscillations. These oscillations are due to the production of debris, that increases the friction coefficient, and are then discharged reducing the friction. Friction coefficients in tests 2 and 4 showed a similar trend that is different from the behavior observed in tests 1 and 3. The friction coefficients increased at the early stages and then gradually leveled off. This behavior was observed also in [8, 15, 22, 23, 32]. As explained in [33], in the early stage the coefficient of friction increases due to a rapid increase in the number of wear particles entrapped between the sliding surfaces. As the wear process go on the frictional force decreases, due to the decrease in asperity deformation and ploughing. The steady state condition is reached when the generation of new wear particles balance the particles leaving the interface and the surface becomes mirror smooth as a result of the wear process. Tests point out the role of the roughness. Surface with higher roughness shows a larger variation of the friction coefficient than surface with lower roughness. Higher asperities are easier to cut by shear loads and larger debris is generated.

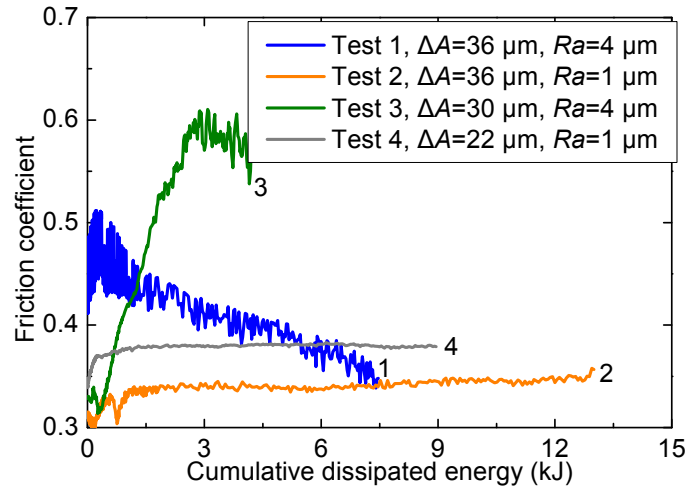


**Fig. 11.** Evolution of friction coefficients with cumulative energy dissipated.

### 3.4 Worn surfaces

Microscopic images of contact surfaces were obtained by a stereomicroscope. Figure 12 shows the photographs of contact surfaces after fretting wear tests. In these images wear scars are surrounded by yellow lines. Wear scars are distributed in different way for different tests. In test 1, the wear scars are some vertical stripes that are evenly distributed along the direction of movement. These stripes coincide with traces of wire cutting. Most likely, the manufacturing process left the contact surface with pronounced waviness. In test 3, the wear scars are mainly found around the through hole, probably because of the protrusion of the hole edges due to the drilling process. In tests 2 and 4, wear scars are mainly distributed near the left border of the contact surfaces, with only a small part on the right. This is probably caused by the hand-polished process.

1004  
1005  
1006  
1007  
1008  
1009  
1010  
1011  
1012  
1013  
1014  
1015  
1016  
1017  
1018  
1019  
1020  
1021  
1022  
1023  
1024  
1025  
1026  
1027  
1028  
1029  
1030  
1031  
1032  
1033  
1034  
1035  
1036  
1037  
1038  
1039  
1040  
1041  
1042  
1043  
1044  
1045  
1046  
1047  
1048  
1049  
1050  
1051  
1052  
1053  
1054  
1055  
1056  
1057  
1058  
1059  
1060  
1061  
1062

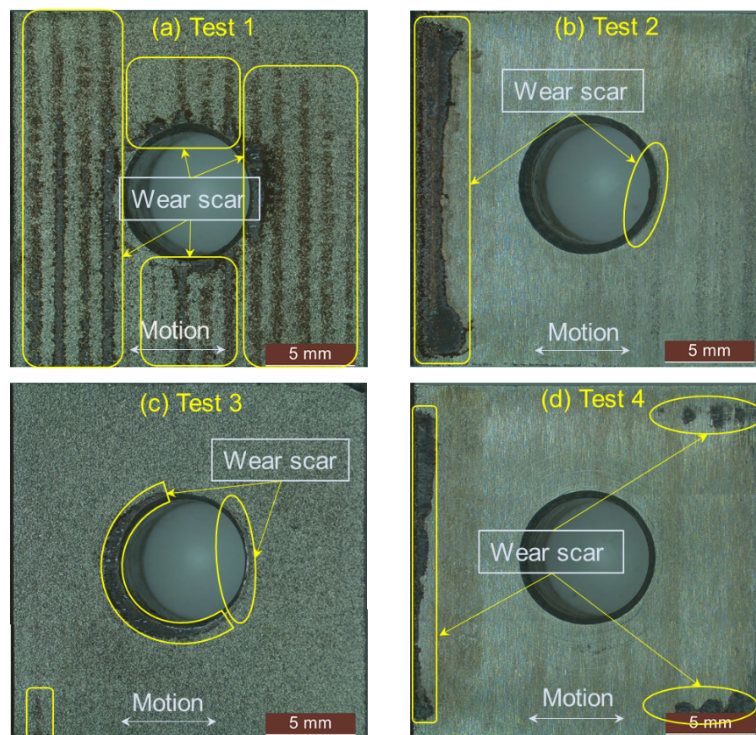


**Fig. 12.** Contact surface images after fretting wear tests, (a) Test 1:  $\Delta x = 50 \mu\text{m}$ ,  $Ra \approx 4 \mu\text{m}$ , (b) Test 2:  $\Delta x = 50 \mu\text{m}$ ,  $Ra \approx 1 \mu\text{m}$ , (c) Test 3:  $\Delta x = 40 \mu\text{m}$ ,  $Ra \approx 4 \mu\text{m}$ , (d) Test 4:  $\Delta x = 40 \mu\text{m}$ ,  $Ra \approx 1 \mu\text{m}$ .

## 4 Modeling wear-induced hysteresis loops evolution

In the past decades, several contact models have been developed to replicate friction hysteresis loops, such as Iwan model [34-36], Bouc-Wen model [37] and LuGre model [38]. In this work, based on the framework of the Iwan model, we introduce parameters that depend on the wear cycles.

### 4.1 Wear-dependent parameters

The Iwan model [36] can be defined by using 3 parameters: tangential contact stiffness  $k_t$ , friction coefficient  $\mu$  and normal preload  $N_b$ . The original Iwan model is not able to simulate the residual stiffness phenomenon, therefore a new parameter, namely the residual stiffness  $k_r$ , was introduced. In this work, the parameters in the Iwan model are formulated as functions of the cumulative dissipated energy  $E$ .

To simulate the evolution of parameters with wear (wear-dependent parameters), a set of exponential basis functions, reported in Table 3, was selected. The coefficients of these basis functions were obtained by fitting the experimental results. The same functions were used for tests 2 and 4. The subscript '0',  $N_{b0}$ ,  $k_{t0}$  and  $\mu_0$ , denotes the initial values of contact parameters. The exponents of the basis functions,  $c$  and  $d$  were the same for different parameters and were obtained through a best fit procedure with the least square method. Results of the best fit procedure showed that these exponents are the same for similar contact conditions, for example tests 2 and 4. Results of the best fit procedure are shown in Table A1 (see Appendix A). Coefficients  $a_i$  ( $i=1, 2, 3$ ) of the basis functions are the ratio between the final value and the initial value of the contact parameter. Coefficients  $b_i$  ( $i=1, 2$ ) are the multiplier of the basis functions and with range  $[0, 1]$ . Details about these coefficients can be found in Appendix A. The residual stiffness was considered independent of wear cycles as it is related to the bending stiffness of the bolt shank that is not affected by the change in bolt preloads [24]. Results in Fig. 13(d) support the above assumption.

Figure 13 shows the wear-dependent parameters of tests 2 and 4 as a function of the energy  $E$  and compares the analytical parameters, as defined in Table 3, with the measured parameters. All coefficients and corresponding standard deviations with 95% confidence bounds can be found in Appendix A. Taking the evolution of bolt preload (in Test 4) as an example, Figure 13 (a) shows the upper and lower limits of the fitting curve considering the coefficient deviation.

**Table 3** Functions of wear-dependent contact parameters

Variables	Functions
Bolt preload	$N_b(E) = N_{b0}[a_1 + (1 - a_1)e^{cE}]$
Contact stiffness	$k_t(E) = k_{t0}\{a_2 + (1 - a_2)[b_1e^{cE} + (1 - b_1)e^{dE}]\}$
Friction coefficient	$\mu(E) = \mu_0\{a_3 + (1 - a_3)[b_2e^{cE} + (1 - b_2)e^{dE}]\}$

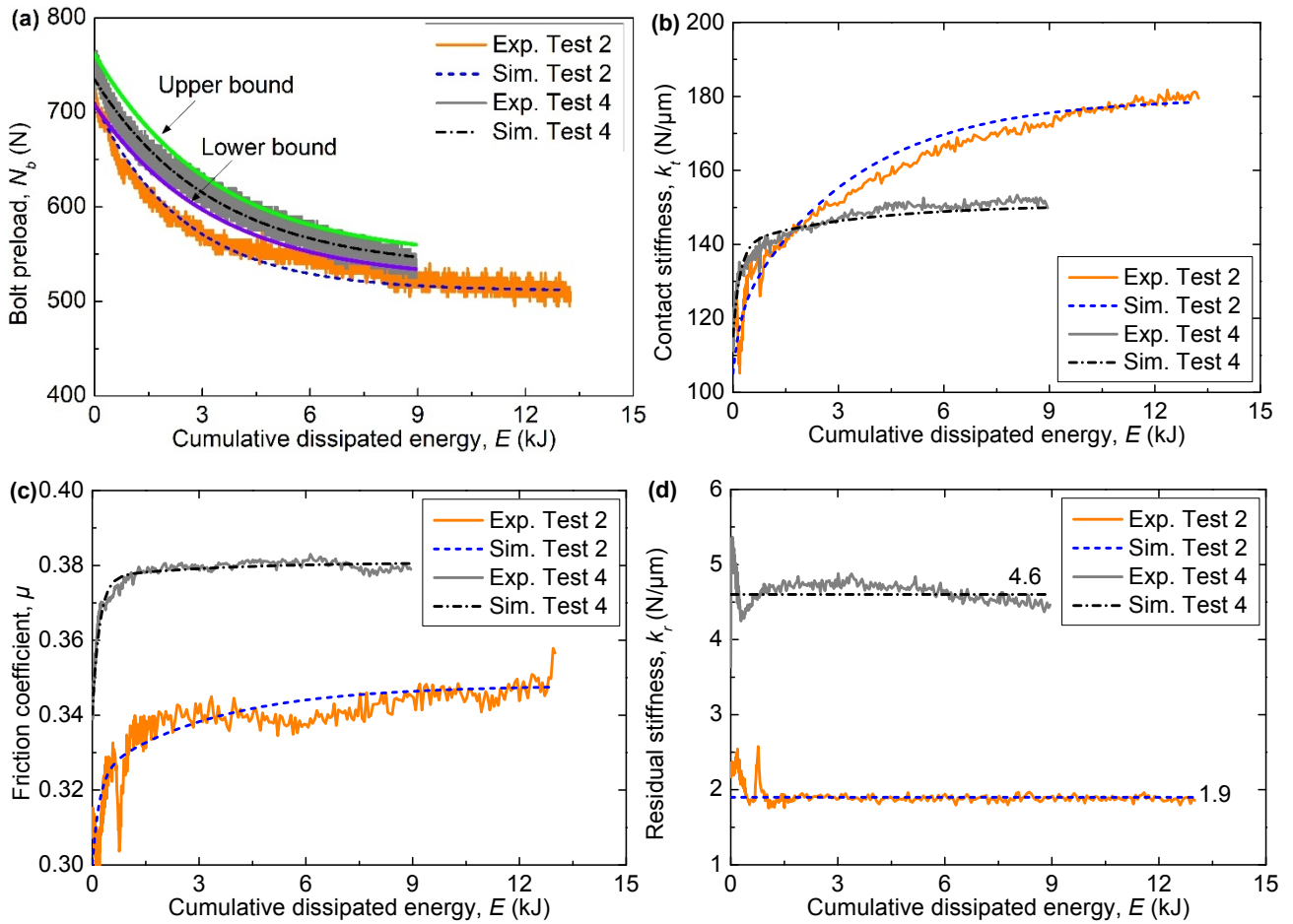


**Fig. 13.** Wear-dependent parameters for tests 2 and 4: (a) Bolt preload; (b) tangential contact stiffness; (c) friction coefficient; (d) residual stiffness.

#### 4.2 Iwan model with wear-dependent parameters

The Iwan model is composed of infinite number of Jinkins elements in parallel. These elements have the same contact stiffness and different critical sliding force. The sum of the critical sliding force on each element is equal to Coulomb friction force  $\mu N_b$  and it is distributed to each element with a

uniform density function. The Iwan model can reproduce stick, micro-slip and gross slip behavior of contact surfaces under tangential vibrations. A detailed description of the Iwan model and its recent improvement for using in modeling joint can be found in [34-36].

The original Iwan model was modified to consider the effect of the residual stiffness. For a monotonic loading case, the force-displacement relationship of the modified Iwan model is written as

$$T_m(\delta) = \begin{cases} (k_t + k_r)\delta - \frac{(k_t\delta)^2}{4\mu N_b}, & \delta < \frac{2\mu N_b}{k_t + k_r} \\ \mu N_b + k_r\delta, & \delta > \frac{2\mu N_b}{k_t + k_r} \end{cases} \quad (2)$$

where  $T_m$  is the tangential force and  $\delta$  the tangential relative displacement. For a cyclic loading case, the force-displacement relationship can be obtained by substituting Eq. (2) into Eq. (3),

$$T(\delta) = \begin{cases} -T_m(\delta_m) + 2T_m\left(\frac{\delta_m + \delta}{2}\right), & \delta > 0 \\ T_m(\delta_m) - 2T_m\left(\frac{\delta_m - \delta}{2}\right), & \delta < 0 \end{cases} \quad (3)$$

where  $T$  is the tangential force and  $\delta_m$  the amplitude of tangential relative displacements.

The wear-dependent parameters are included in the modified Iwan model to simulate the effect of wear on the friction behavior. The resulting force-displacement relationship for monotonic loading case is

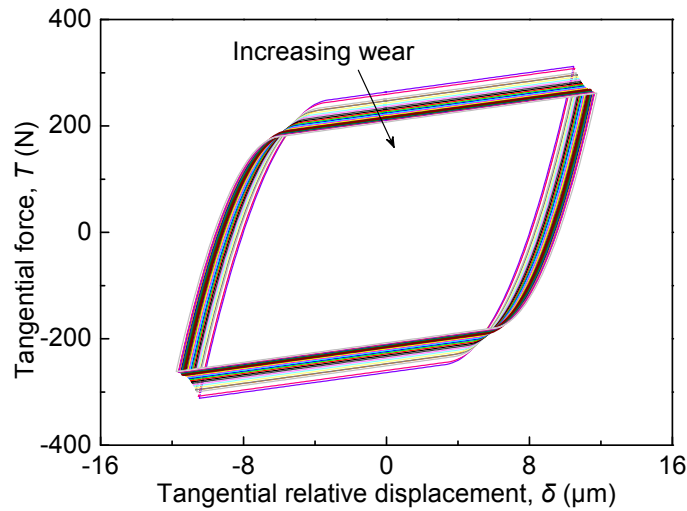
$$T_m(\delta, E) = \begin{cases} [k_t(E) + k_r(E)]\delta - \frac{[k_t(E)\delta]^2}{4\mu(E)N_b(E)}, & \delta < \frac{2(E)N_b(E)}{k_t(E) + k_r(E)} \\ \mu(E)N_b(E) + k_r(E)\delta, & \delta > \frac{2(E)N_b(E)}{k_t(E) + k_r(E)} \end{cases} \quad (4)$$

Substituting Eq. (4) into Eq. (3) yields the force-displacement relationship for the cyclic loading case. In Eq. (4) there are two independent variables, namely  $\delta$  and  $E$ , that have different time scales. The cumulative dissipated energy is defined over one period of vibration and it is a step function in the time function. In the process of calculating hysteresis loops the step size of the cumulative dissipated energy  $E$  is the period of vibration.

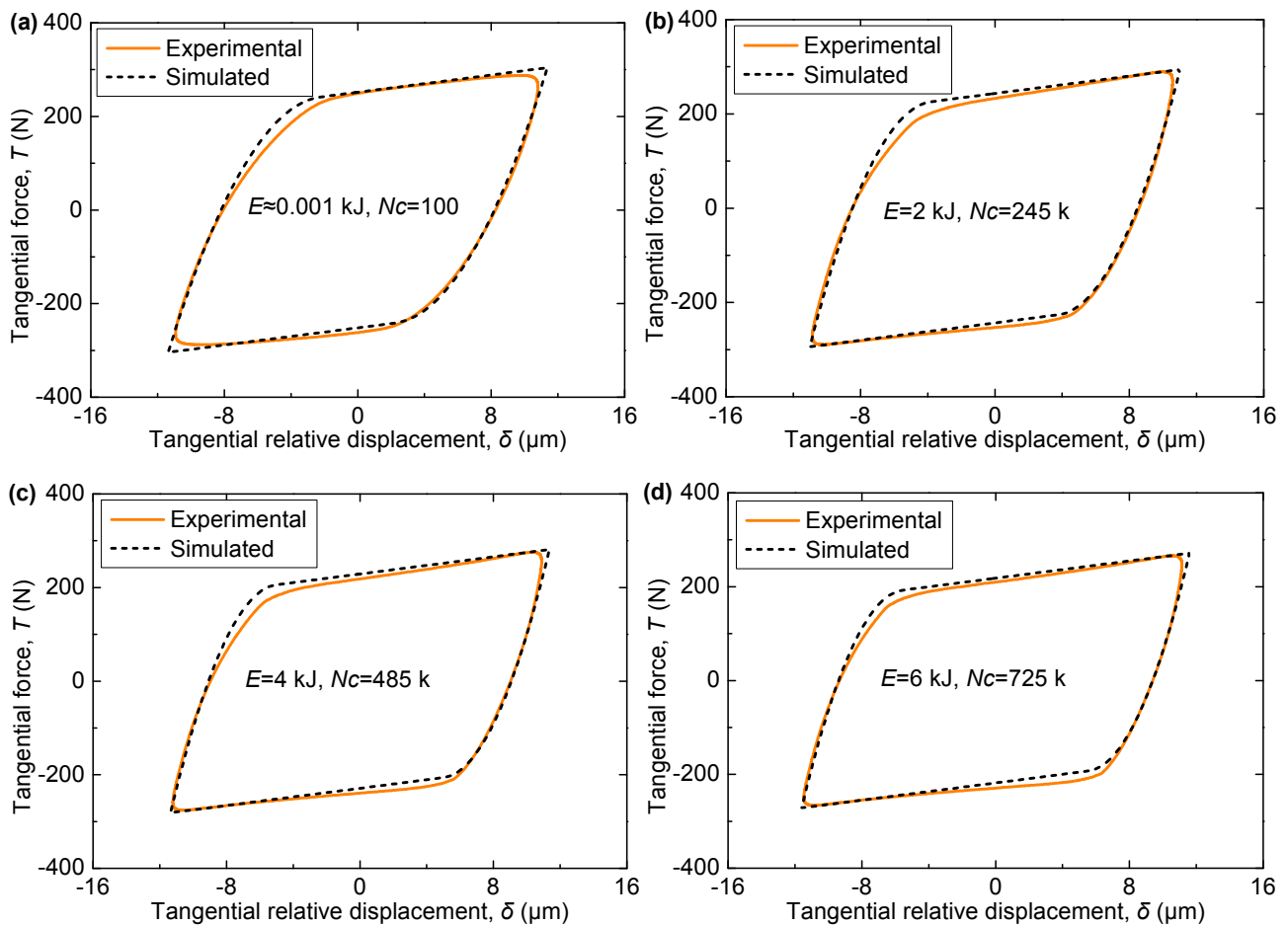
After each vibration period, the cumulative dissipated energy is recalculated. Then the contact parameters are updated for the next vibration period. Performing this operation cyclically results in the

1240  
 1241  
 1242  
 1243 hysteresis loops involving wear evolution. Figure 14 depicts the evolution of the hysteresis loops with  
 1244 increasing wear simulated by the proposed method.

1245  
 1246  
 1247 To assess the effectiveness of the proposed method, a set of simulated results were compared with  
 1248 the experimental counterparts. Figure 15 shows the results of the comparison that are in good  
 1249 agreement with the measured hysteresis loops.  
 1250  
 1251



1252  
 1253  
 1254  
 1255  
 1256  
 1257  
 1258  
 1259  
 1260  
 1261  
 1262  
 1263  
 1264  
 1265  
 1266  
 1267 **Fig. 14.** Evolution of simulated hysteresis loops with increasing wear for test 4.  
 1268



1269  
 1270  
 1271  
 1272  
 1273  
 1274  
 1275  
 1276  
 1277  
 1278  
 1279  
 1280  
 1281  
 1282  
 1283  
 1284  
 1285  
 1286  
 1287  
 1288  
 1289  
 1290  
 1291  
 1292  
 1293  
 1294  
 1295  
 1296  
 1297  
 1298

1299  
1300  
1301  
1302  
1303  
1304  
1305  
1306  
1307  
1308  
1309  
1310  
1311  
1312  
1313  
1314  
1315  
1316  
1317  
1318  
1319  
1320  
1321  
1322  
1323  
1324  
1325  
1326  
1327  
1328  
1329  
1330  
1331  
1332  
1333  
1334  
1335  
1336  
1337  
1338  
1339  
1340  
1341  
1342  
1343  
1344  
1345  
1346  
1347  
1348  
1349  
1350  
1351  
1352  
1353  
1354  
1355  
1356  
1357

**Fig. 15.** Comparison between simulated and experimental hysteresis loops in test 4: (a)  $E \approx 1\text{J}$ ,  $N_c=100$ ; (b)  $E = 2\text{kJ}$ ,  $N_c=245\text{k}$ ; (c)  $E = 4\text{kJ}$ ,  $N_c=485\text{k}$ ; (d)  $E = 6\text{kJ}$ ,  $N_c=725\text{k}$ .  $N_c$  is the number of wear cycle.



## 5 Conclusions

Prior works have documented how fretting wear influenced the contact parameters and the dynamic behavior of structures. These early studies did not consider the interaction between fretting wear and bolt preload. This work investigated the fretting wear behavior of bolted joint interfaces. Tests were performed with an apparatus specifically designed to measure the friction hysteresis behavior of bolted joint. The tangential contact force and the relative displacements were measured at different stages of wear. Contact parameters, tangential stiffness and friction coefficient, were extracted from the hysteresis loops and their evolution monitored with wear cycles. Bolt preloads were also recorded continuously during the tests.

Experimental results showed that the surface roughness significantly influenced the evolution of the contact parameters. For the same sliding amplitude, the higher the surface roughness, the more drastic the change in the shape of the hysteresis loop. Hysteresis loops on rough surfaces showed a residual stiffness that gradually decreases with wear cycles. Moreover, the tangential force decreased with the wear cycles and the gross slip regime became predominant. The preload decreased with wear cycles as well and since the tangential force is related to the bolt preload the two results are consistent. Preload on rough surface at the end of the test was 10% of the initial preload. Smooth surfaces showed a reduction in the preload that was much less than that of the rough surfaces. Higher asperities are easily deformed or cut, and these processes led to reduction of the interference fit between the connected part, which in turn resulted in reduction of the bolt preload.

The contact stiffness is mainly driven by the true contact area that in turn increases with the normal load. Since the contact stiffness increased with decreasing the preload, this is a clear evidence that the increase in the contact area due to the wear process overcame the decrease in contact area due to the decrease in the preload. Contact stiffness for rough surfaces showed a peak when the preload becomes very low. Preload on smooth surfaces did not reach such low values of preload and a comparison is not possible.

The friction coefficient of rough and smooth surfaces showed a remarkable different behavior. The friction coefficient of smooth surfaces increased and then levelled off. On the other hand, the

1417  
1418  
1419  
1420 friction coefficient of rough surface increased up to a peak, decreased and then levelled off. For the  
1421  
1422 rough surfaces, the wear process is more prone to produce wear particles. Wear particles entrapped in  
1423  
1424 the contact surfaces are the main reason for the increase in friction coefficient in the early state of wear.  
1425  
1426 When debris generated by the wear process balance the debris ejected outside the contact, the friction  
1427  
1428 coefficient stabilized towards a steady-state value.

1429  
1430 In this study, a contact model was developed to simulate the fretting wear behavior of bolted joint  
1431  
1432 interfaces. This method reconstructs the evolution of contact parameters using a set of wear-dependent  
1433  
1434 coefficients. Dependence on wear was formulated in terms of cumulative dissipated energy. These  
1435  
1436 coefficients were introduced in the well-known Iwan model to replicate the evolution of hysteresis  
1437  
1438 loops with wear. The simulated and measured hysteresis loops were in good agreement and prove the  
1439  
1440 reliability of the proposed numerical method. It should be noted that the proposed wear-dependent  
1441  
1442 coefficients can also be combined with other contact models. The developed method can be used to  
1443  
1444 simulate the dynamics of bolted joint structures in which fretting wear process heavily alters the  
1445  
1446 contact conditions.  
1447  
1448  
1449  
1450  
1451  
1452  
1453  
1454  
1455  
1456  
1457  
1458  
1459  
1460  
1461  
1462  
1463  
1464  
1465  
1466  
1467  
1468  
1469  
1470  
1471  
1472  
1473  
1474  
1475

## Acknowledgments

The authors wish to acknowledge and thank the China Science Challenge for funding their research project (TZ2018007). Dongwu Li would also like to show his gratitude to China Scholarship Council (CSC) for supporting him as a visiting Ph.D. to AERMEC lab of Politecnico di Torino within the project EXTHENdED.

## Appendix A: Coefficients of wear functions

Table A1 lists the parameters of wear functions developed in section 4.1. Table 2 lists the values of all fitted coefficients and their standard deviations with 95% confidence bounds. The coefficient  $a_i$  ( $i = 1, 2, 3$ ) is defined as the ratio of the final value of contact parameters to the initial value. The coefficients  $c$  and  $d$  are the exponents of the basis function. Tests 2 and 4 have the same coefficients  $a_i$ ,  $c$  and  $d$ . The coefficient  $b_i$  ( $i = 1, 2$ ) is the multiplier of the basis function and is in the range  $[0, 1]$ .

**Table A1** Parameters of wear functions

Variables	Test 2	Test 4
Bolt preload	$N_{b0}=710$ N, $c = -0.3$	$N_{b0}=745$ N, $c = -0.3$
Contact stiffness	$k_{t0}=105$ N/ $\mu\text{m}$ , $c = -0.3$ , $d = -5$	$k_{t0}=115$ N/ $\mu\text{m}$ , $c = -0.3$ , $d = -5$
Friction coefficient	$\mu_0=0.3$ , $c = -0.3$ , $d = -5$	$\mu_0=0.34$ , $c = -0.3$ , $d = -5$

**Table A2** Fitted coefficients and its standard deviations with 95% confidence bounds

Coefficients	Values with 95% confidence bounds			
	Test 2	Test 4	Test 2	Test 4
$a_1$	0.72	0.72	$\pm 0.040$	$\pm 0.031$
$a_2$	1.71	1.31	$\pm 0.003$	$\pm 0.003$
$a_3$	1.16	1.12	$\pm 0.012$	$\pm 0.010$
$b_1$	0.4	0.8	$\pm 0.015$	$\pm 0.020$
$b_2$	0.2	0.5	$\pm 0.019$	$\pm 0.014$

## References

- [1] A. Ferjaoui, T. Yue, M.A. Wahab, R. Hojjati-Talemi, Prediction of fretting fatigue crack initiation in double lap bolted joint using Continuum Damage Mechanics, *International Journal of Fatigue*, 73 (2015) 66-76. <https://doi.org/10.1016/j.ijfatigue.2014.11.012>.
- [2] J. Juoksukangas, A. Lehtovaara, A. Mantyla, Experimental and numerical investigation of fretting fatigue behavior in bolted joints, *Tribology International*, 103 (2016) 440-448. <https://doi.org/10.1016/j.triboint.2016.07.021>.
- [3] C. Jimenez-Pena, R.H. Talemi, B. Rossi, D. Debruyne, Investigations on the fretting fatigue failure mechanism of bolted joints in high strength steel subjected to different levels of pre-tension, *Tribology International*, 108 (2017) 128-140. <https://doi.org/10.1016/j.triboint.2016.11.014>.
- [4] L. Gaul, R. Nitsche, The Role of Friction in Mechanical Joints, *Applied Mechanics Reviews*, 54 (2001) 93-106. <https://doi.org/10.1115/1.3097294>.
- [5] M.R.W. Brake, et al. *The Mechanics of Jointed Structures: Recent Research and Open Challenges for Developing Predictive Models for Structural Dynamics*. Springer, 2017. <https://doi.org/10.1007/978-3-319-56818-8>.
- [6] D. Botto, M. Lavella, A numerical method to solve the normal and tangential contact problem of elastic bodies, *Wear*, 330-331 (2015) 629-635. <https://doi.org/10.1016/j.wear.2015.02.046>.
- [7] E. Lemoine, D. Nélias, F. Thouverez, C. Vincent, Influence of fretting wear on bladed disks dynamic analysis, *Tribology International*, 145 (2020) 106148. <https://doi.org/10.1016/j.triboint.2019.106148>.
- [8] A. Fantetti, L.R. Tamatam, M. Volvert, I. Lawal, L. Liu, L. Salles, M.R.W. Brake, C.W. Schwingshackl, D. Nowell, The impact of fretting wear on structural dynamics: Experiment and Simulation, *Tribology International*, 138 (2019) 111-124. <https://doi.org/10.1016/j.triboint.2019.05.023>.
- [9] L. Salles, L. Blanc, F. Thouverez, A.M. Gousskov, Dynamic analysis of fretting-wear in friction contact interfaces, *International Journal of Solids and Structures*, 48 (2011) 1513-1524. <https://doi.org/10.1016/j.ijsolstr.2011.01.035>.
- [10] J. Armand, L. Pesaresi, L. Salles, C.W. Schwingshackl, A Multiscale Approach for Nonlinear Dynamic Response Predictions With Fretting Wear, *Journal of Engineering for Gas Turbines and Power*, 139 (2017) 022505. <https://doi.org/10.1115/1.4034344>.
- [11] Y. Yoon, I. Etsion, F.E. Talke, The evolution of fretting wear in a micro-spherical contact, *Wear*, 270 (2011) 567-575. <https://doi.org/10.1016/j.wear.2011.01.013>.
- [12] M.R. Hirsch, R.W. Neu, A simple model for friction evolution infretting, *Wear*, 301 (2013) 517-523. <https://doi.org/10.1016/j.wear.2013.01.036>.
- [13] T. Liskiewicz, S. Fouvry, Development of a friction energy capacity approach to predict the surface coating endurance under complex oscillating sliding conditions, *Tribology International*, 38 (2005) 69-79. <https://doi.org/10.1016/j.triboint.2004.06.002>.
- [14] M. Eriten, A.A. Polycarpou, L.A. Bergman, Effects of surface roughness and lubrication on the early stages of fretting of mechanical lap joints, *Wear*, 271 (2011) 2928-2939. <https://doi.org/10.1016/j.wear.2011.06.011>.
- [15] M. Lavella, D. Botto, M.M. Gola, Design of a high-precision, flat-on-flat fretting test apparatus

- 1653  
1654  
1655 with high temperature capability, *Wear*, 302 (2013) 1073-1081.  
1656 <https://doi.org/10.1016/j.wear.2013.01.066>.  
1657  
1658 [16] Botto D, Campagna A, Lavella M, Gola, MM. Experimental and numerical investigation of  
1659 fretting wear at high temperature for aeronautical alloys. *Proceedings of the ASME Turbo Expo*. 2010;  
1660 6: 1353-1362. <https://doi.org/10.1115/GT2010-23356>.  
1661  
1662 [17] M. Lavella, D. Botto, Fretting Fatigue Analysis of Additively Manufactured Blade Root Made of  
1663 Intermetallic Ti-48Al-2Cr-2Nb Alloy at High Temperature, *Materials*, 11 (2018). <https://doi.org/10.3390/ma11071052>.  
1664  
1665 [18] M. Lavella, D. Botto, Fretting wear characterization by point contact of nickel superalloy  
1666 interfaces, *Wear*, 271 (2011) 1543-1551. <https://doi.org/10.1016/j.wear.2011.01.064>.  
1667  
1668 [19] M.E. Kartal, D.M. Mulvihill, D. Nowell, D.A. Hills, Measurements of pressure and area  
1669 dependent tangential contact stiffness between rough surfaces using digital image correlation,  
1670 *Tribology International*, 44 (2011) 1188-1198. <https://doi.org/10.1016/j.triboint.2011.05.025>.  
1671  
1672 [20] D.M. Mulvihill, M.E. Kartal, A.V. Olver, D. Nowell, D.A. Hills, Investigation of non-Coulomb  
1673 friction behaviour in reciprocating sliding, *Wear*, 271 (2011) 802-816. <https://doi.org/10.1016/j.wear.2011.03.014>.  
1674  
1675 [21] K.J. Kubiak, T.G. Mathia, S. Fouvry, Interface roughness effect on friction map under fretting  
1676 contact conditions, *Tribology International*, 43 (2010) 1500-1507. <https://doi.org/10.1016/j.triboint.2010.02.010>.  
1677  
1678 [22] J. Hintikka, A. Lehtovaara, A. Mäntylä, Fretting-induced friction and wear in large flat-on-flat  
1679 contact with quenched and tempered steel, *Tribology International*, 92 (2015) 191-202. <https://doi.org/10.1016/j.triboint.2015.06.008>.  
1680  
1681 [23] C.W. Schwingshackl, E.P. Petrov, D.J. Ewins, Measured and estimated friction interface  
1682 parameters in a nonlinear dynamic analysis, *Mechanical Systems and Signal Processing*, 28 (2012)  
1683 574-584. <https://doi.org/10.1016/j.ymssp.2011.10.005>.  
1684  
1685 [24] Li D., Xu C., Botto D., et. al. A novel test apparatus for measuring friction hysteresis of bolted  
1686 joints, *Tribology International*, 2020, Under review.  
1687  
1688 [25] H. Gong, J. Liu, X. Ding, Study on the mechanism of preload decrease of bolted joints subjected  
1689 to transversal vibration loading, *Proceedings of the Institution of Mechanical Engineers, Part B: Journal of Engineering Manufacture*, 233 (2019) 2320-2329. <https://doi.org/10.1177/0954405419838675>.  
1690  
1691 [26] Y. Jiang, M. Zhang, C.-H. Lee, A Study of Early Stage Self-Loosening of Bolted Joints, *Journal of Mechanical Design*, 125 (2003) 518-526. <https://doi.org/10.1115/1.1586936>.  
1692  
1693 [27] R.I. Zadoks, X. Yu, An investigation of the self-loosening behavior of bolts under transverse  
1694 vibration, *Journal of Sound and Vibration*, 208 (1997) 189-209. <https://doi.org/10.1006/jsvi.1997.1173>.  
1695  
1696 [28] D. Botto, M. Lavella, High temperature tribological study of cobalt-based coatings reinforced  
1697 with different percentages of alumina, *Wear*, 318 (2014) 89-97. <https://doi.org/10.1016/j.wear.2014.06.024>.  
1698  
1699 [29] S. Fouvry, P. Duó, P. Perruchaut, A quantitative approach of Ti-6Al-4V fretting damage: friction,  
1700 wear and crack nucleation, *Wear*, 257 (2004) 916-929. <https://doi.org/10.1016/j.wear.2004.05.011>.  
1701  
1702 [30] M. Gonzalez-Valadez, A. Baltazar, R.S. Dwyer-Joyce, Study of interfacial stiffness ratio of a  
1703 rough surface in contact using a spring model, *Wear*, 268 (2010) 373-379. <https://doi.org/10.1016/j.wear.2010.03.014>.  
1704  
1705  
1706  
1707  
1708  
1709  
1710  
1711

1712  
1713  
1714 [wear.2009.08.022.](https://doi.org/10.1007/978-1-4613-8865-4_32)

1715  
1716 [31] R.D. Mindlin, W.P. Mason, T.F. Osmer, et al. Effects of an oscillating tangential force on the  
1717 contact surfaces of elastic spheres. *J. Appl. Mech.* 18 (1951) 331-331. [https://doi.org/ 10.1007/978-1-](https://doi.org/10.1007/978-1-4613-8865-4_32)  
1718 [4613-8865-4\\_32.](https://doi.org/10.1007/978-1-4613-8865-4_32)

1719 [32] M.E. Kartal, D.M. Mulvihill, D. Nowell, D.A. Hills, Determination of the Frictional Properties of  
1720 Titanium and Nickel Alloys Using the Digital Image Correlation Method, *Experimental Mechanics*,  
1721 51 (2011) 359-371. [https://doi.org/10.1007/s11340-010-9366-y.](https://doi.org/10.1007/s11340-010-9366-y)

1722 [33] N.P. Suh, H.C. Sin, The genesis of friction. *Wear*, 69(1) (1981) 91-114. [https://doi.org/10.1016/](https://doi.org/10.1016/0043-1648(81)90315-X)  
1723 [0043-1648\(81\)90315-X.](https://doi.org/10.1016/0043-1648(81)90315-X)

1724 [34] W.D. Iwan, A Distributed-Element Model for Hysteresis and Its Steady-State Dynamic Response,  
1725 *Journal of Applied Mechanics*, 33 (1966) 893-900. [https://doi.org/10.1115/1.3625199.](https://doi.org/10.1115/1.3625199)

1726 [35] D. Li, D. Botto, C. Xu, T. Liu, M. Gola, A micro-slip friction modeling approach and its  
1727 application in underplatform damper kinematics, *International Journal of Mechanical Sciences*, 161-  
1728 162 (2019) 105029. [https://doi.org/10.1016/j.ijmecsci.2019.105029.](https://doi.org/10.1016/j.ijmecsci.2019.105029)

1729 [36] D. Li, C. Xu, T. Liu, M.M. Gola, L. Wen, A modified IWAN model for micro-slip in the context  
1730 of dampers for turbine blade dynamics, *Mechanical Systems and Signal Processing*, 121 (2019) 14-  
1731 30. [https://doi.org/10.1016/j.ymsp.2018.11.002.](https://doi.org/10.1016/j.ymsp.2018.11.002)

1732 [37] F. Ikhouane, J. Rodellar, On the Hysteretic Bouc–Wen Model, *Nonlinear Dynamics*, 42 (2005)  
1733 63-78. [https://doi.org/10.1007/s11071-005-0069-3.](https://doi.org/10.1007/s11071-005-0069-3)

1734 [38] K. Johansson, C. Canudas-de-Wit, Revisiting the LuGre friction model, *IEEE Control Systems*  
1735 *Magazine*, 28 (2008) 101-114. [https://doi.org/10.1109/MCS.2008.929425.](https://doi.org/10.1109/MCS.2008.929425)

1741  
1742  
1743  
1744  
1745  
1746  
1747  
1748  
1749  
1750  
1751  
1752  
1753  
1754  
1755  
1756  
1757  
1758  
1759  
1760  
1761  
1762  
1763  
1764  
1765  
1766  
1767  
1768  
1769  
1770